ACS Photonics

Letter

pubs.acs.org/journal/apchd5

Coupling Quantum Emitters in 2D Materials with Tapered Fibers

Andreas W. Schell,*[,†] Hideaki Takashima,[†] Toan Trong Tran,[‡] Igor Aharonovich,[‡] and Shigeki Takeuchi*[,†]

[†]Department of Electronic Science and Engineering, Kyoto University, 615-8510 Kyoto, Japan

[‡]School of Mathematical and Physical Sciences, University of Technology Sydney, Ultimo, New South Wales 2007, Australia

ABSTRACT: Realization of integrated photonic circuits on a single chip requires controlled manipulation and integration of solid-state quantum emitters with nanophotonic components. Previous works focused on emitters embedded in a three-dimensional crystal, such as nanodiamonds or quantum dots. In contrast, in this work we demonstrate coupling of a single emitter in a two-dimensional (2D) material, namely, hexagonal boron nitride, with a tapered optical fiber and find a collection efficiency of the system of 10%. Furthermore, due to the single dipole character of the emitter, we were able to analyze the angular emission pattern of the coupled system via back focal plane imaging. The good coupling efficiency to the tapered fiber even allows excitation and detection in a fully fiber coupled way, yielding a true integrated system. Our results provide evidence of the feasibility to efficiently integrate quantum emitters in 2D materials with photonic structures.

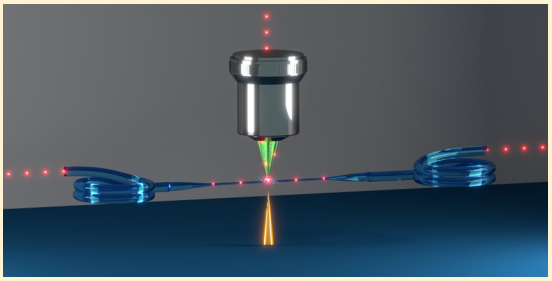

KEYWORDS: *2D materials, hexagonal boron nitride, single-photon emitters, tapered fiber, nanofiber*

Atomically thin two-dimensional (2D) materials are garnering major attention in a variety of emerging applications in nanophotonics and optoelectronics[1,2] spanning low threshold lasing,[3] subdiffraction imaging,[4,5] valleytronics,[6,7] and efficient light-emitting diodes.[8,9] In particular, hexagonal boron nitride (hBN) has recently emerged as a promising layered material that hosts optically stable single-photon emitters that operate at room temperature.[10−13] These defects have a narrow emission line width from the ultraviolet to the near-infrared spectral range, are bright, and can be excited by two-photon excitation.[14] These properties make them promising candidates for applications in (bio)-sensing,[15] nanophotonics,[16] and quantum information science.[17]

However, in order to employ these emitters in applications, e.g., as single-photon sources, it is necessary to efficiently extract the emitted photons.[18] While usage of solid immersion lenses[19] and dielectric antennas[20] has been demonstrated, these approaches do not offer a path to scalability and suffer from complicated output modes. A promising direction to overcome this problem is using near-field coupling to tapered optical fibers,[21−23] where the photons get directly emitted into a guided mode inside the fiber. In these geometries, coupling efficiencies of over 20% can be reached, and even higher efficiencies are possible by combining the tapered fibers with optical cavities, such as nanofiber Bragg cavities (NFBCs).[24−26] Because photon collection and excitation of the emitter in such a system can be performed using different spatial modes—free space and the fiber—it can be used to separate excitation light from fluorescence in resonance fluorescence experiments.

In this Letter, we demonstrate unprecedented results of coupling quantum emitters embedded in layered hBN to a tapered optical fiber. We show efficient collection of light emitted by a single-photon emitter into the optical fiber and prove that the quantum nature of light is maintained throughout when the light is guided through the fiber. We further analyze the collection efficiency in detail by taking into account the nonisotropic emission of a dipole emitter.

A sketch of the setup is shown in Figure 1 (see Methods for detailed description). The setup consists of a home-built beam-scanning confocal microscope equipped with a spectrometer and avalanche photodiodes for photon correlation measurements. The emitters in hBN (see Methods) are excited using pulsed or continuous wave lasers at a wavelength of 532 nm. A tapered optical fiber with a radius of 320 nm is positioned in front of the objective lens with a numerical aperture (NA) of 0.95. One end of the fiber is spliced to a longer fiber, from which the light is coupled out in order to perform filtering before it is sent to the detectors.

To transfer the hBN flakes that host the quantum emitters onto the tapered fiber, a sharp tungsten tip driven by a piezo positioner is used.[27] The hBN flakes are lifted off the silicon substrate with the tip. Subsequently, the flakes are then placed onto the fiber by approaching the tungsten tip to the tapered region of the fiber. After successful transfer of an hBN flake, room-temperature optical measurements were carried out.

We first compare the emission properties of the hBN sources into free space using the high-NA objective lens with the collection through the fiber. Figure 2a and b show the room-temperature spectra of the light collected through the objective lens and through the fiber, respectively. In both spectra, two

Received: January 10, 2017
Published: March 10, 2017

DOI: 10.1021/acsphotonics.7b00025
ACS Photonics 2017, 4, 761−767

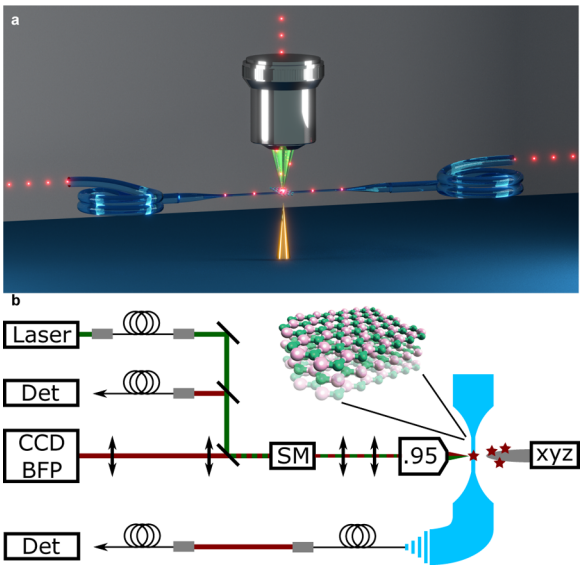

Figure 1. Setup used in the experiment. (a) Illustration of the experiment. (b) The setup used in this experiment consists of a home-built confocal microscope equipped with a piezo-driven three-axis manipulator (*xyz*) for attaching hBN flakes to a tapered optical fiber (colored blue). The microscope uses an objective lens with a numerical aperture of 0.95, and raster scanning is achieved using a scanning mirror assembly (SM). Different lasers (pulsed or cw) can be fiber coupled to the microscope, and detection occurs via either a CCD camera for imaging the sample or the back focal plane (BFP) of the objective. Detection (Det) of the light is done with interchangeable modules for registering intensity, spectrum, and intensity correlations. Fiber coupling of the modules makes their use with the microscope as well as with the fiber possible. Light inside the fiber is coupled out for filtering and then coupled to another fiber and sent to the detection units (Det). hBN flakes are depicted in the rendering (rose is boron, green is nitrogen) and as stars.

peaks are visible (at 573 and 666 nm), most likely corresponding to two individual single emitters. In the following, the emitter at 666 nm will be investigated in detail. Unless otherwise stated, a bandpass filter between 650 and 700 nm is used. The full width at half-maximum (fwhm) of the peak is approximately 2 nm. Notably, in both cases, namely, through the fiber and via the high-NA objective, the spectra are very similar, and the sharp lines of the emitter are clearly visible. The minor differences can be explained by different coupling efficiencies to the fiber and the objective lens and by fluorescence coming from pump light entering the silica fiber.

To prove that the emitter is indeed a single-photon source, the second-order autocorrelation function, $g^{(2)}(t)$, is recorded. Figure 2c and d show these antibunching measurements of the light collected through the objective lens and through the fiber's end, respectively. The measurements were carried out using the 10 nm bandpass filter in order to only collect light from the sharp line at 666 nm. Both curves show a pronounced dip at zero time delay ($t = 0$), confirming the single-photon nature of the light. This clearly proves that the coupling of a defect in a two-dimensional material to the fiber and extraction of its photons are successful.

In Figure 2e lifetime measurements for the free space collection and collection via the fiber are shown. The lifetimes through the objective and the fiber are 19.7 and 19.4 ns, respectively. As expected, these lifetimes are nearly identical, as it is the same emitter. The small differences can again be explained by different contributions of background light. To avoid most of these contributions, the fit was carried out to the data starting from 5 ns after the excitation laser pulse.

Finally, we analyze the temporal stability of this emitter by recording the intensity count rate as a function of time. The corresponding measurements are shown in Figure 2f. As expected, the emission is modulated in a very similar manner when collected via both outputs, namely, air objective (upper part) and fiber (lower part). The observed sharp steps in both cases are an indication that this modulation is not caused by the fiber vibrating and drifting through the laser focus, where the modulation would be expected to be continuous. This indicates a blinking behavior of the emitter, which was also found for some, but not all, emitters on the substrate.

To show the high coupling efficiency of the quantum emitter to the fiber, saturation measurements were carried out (see Figure 3a–c). The saturation curves follow the equation[28]

$$R = R_{\mathrm{inf}} \frac{\left(\frac{I}{I_s}\right)}{\left(\frac{I}{I_s}\right) + 1} + \mathrm{BG} \times I \tag{1}$$

with the pump laser intensity I, the emission rate at saturation R_{inf}, the saturation intensity I_s, and an additional linear background with coefficient BG. From fits to the data saturated emission rates of $R_{\mathrm{inf,obj}}$ = 118 kcounts/s and $R_{\mathrm{inf,fib}}$ = 36 kcounts/s were found for collection through the objective lens and one end of the fiber, respectively. For the fit to the confocal data, due to the higher noise, the saturation intensity was fixed to $I_{\mathrm{s,obj}}$ = 86 μW, which is the value extracted from the fit to the data through the fiber, which exhibits lower noise levels.

The saturation count rates found here are lower than what would be expected from the lifetime of the emitter and the efficiency of the photon collection setup (see below and the Methods section). The cause of this is a nonunity quantum efficiency of the emitter, which leads to fewer photons being emitted.

Since the measurements for the count rate at the tapered fiber were carried out only on one end, in order to exclude reflections in the open end of the fiber, the reflectivity of the whole fiber (including the reflection from the facet) was measured. A value for the reflectivity below 0.1 was found, indicating that this is not the case and the measured count rate stems indeed from the photons emitted in one end.

Figure 3c shows the emission spectrum, excited with a laser beam that is propagating through the fiber. In this configuration, the propagating laser beam can excite background fluorescence inside the fiber, which most likely stems from defects and doping in the fiber itself. Nevertheless, due to a high coupling efficiency for excitation and emitted photons, and the use of a pure silica core tapered fiber, the defect's emission can be detected as a bright line at 666 nm. Excitation and detection through the fiber will enable the system to serve as an integrated single-photon source in quantum networks.

Figure 3d shows the results of numerical simulations of the coupling efficiency for a dipole oriented longitudinal along the fiber, yielding an efficiency of 14.2% for the fiber diameter used in the experiment.

To get more insight into the coupling of the hBN defect to the nanofiber, we performed measurements of the polarization dependence of excitation and emission. The corresponding measurements are shown in Figure 4a–c. In Figure 4a,b, the polarization of the excitation laser is rotated and the emission

DOI: 10.1021/acsphotonics.7b00025
ACS Photonics 2017, 4, 761–767

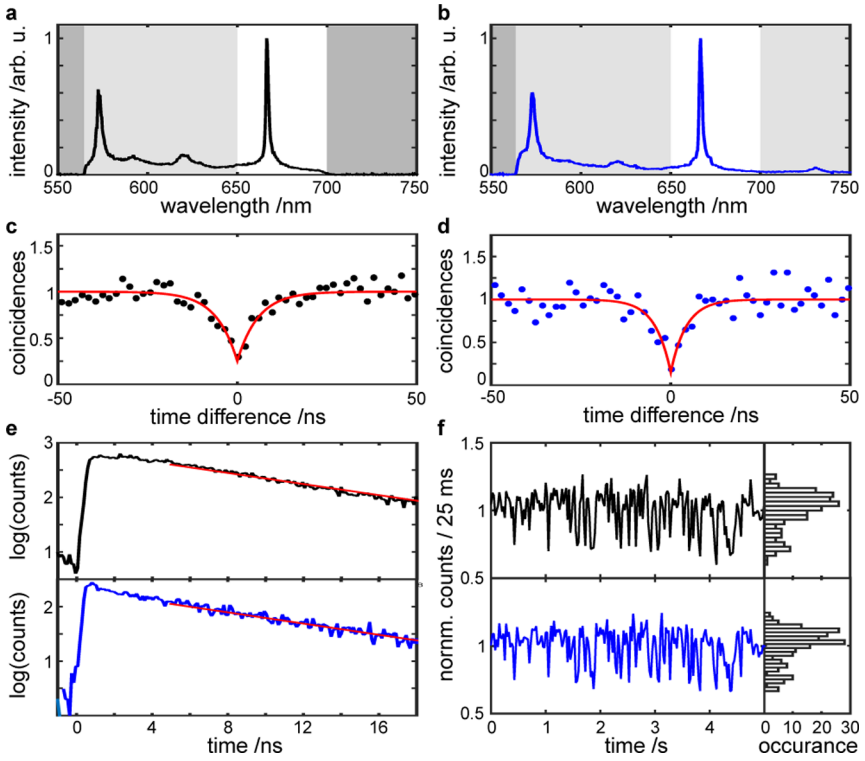

Figure 2. Characterization of a deposited hBN flake. (a, b) Spectrum of the light collected through the microscope objective and the fiber, respectively. Dark gray wavelength ranges are blocked by filters. In the measurements in panel f the light gray ranges are also blocked. For measurements in the other panels, a 10 nm bandpass filter was used to suppress all light but the light coming from the peak at 666 nm. (c, d) Antibunching measurements of the light collected through the objective and through one end of the fiber, respectively. The pronounced dips at zero time delay prove the single-photon nature of the light. Values at zero time difference as extracted from the fits (red lines) are $g^{(2)}(0) = 0.24 \pm 0.11$ and $g^{(2)}(0) = 0.15 \pm 0.20$ through objective and fiber, respectively. Errors are derived from the confidence of the fits to the data. (e) Lifetime measurements through the objective (upper part) and through the fiber end (lower part). Fits to the data (red line) yield lifetimes of 19.7 and 19.4 ns, respectively. (f) Intensity through the objective (upper part) and through the fiber's end (lower part) measured at the same time. A blinking behavior is visible. Note the near-perfect correlation between the blinking in the upper and lower trace.

collected through the objective and through the fiber, respectively. The observed pattern suggests that the transition dipole excited by the laser lies in parallel with the nanofiber. Figure 4c shows the polarization of the photons collected through the objective when the pump laser is coupled into the fiber (i.e., exciting the defect through the fiber). Here, the polarization has a reduced visibility, which could be an indication that the line at 666 nm is excited indirectly.[12]

By coupling single-photon emitters to photonic structures, such as the nanofiber used here, not only are new decay channels provided, but also the overall emission pattern is altered. This can be investigated by imaging the back focal plane (BFP) of the microscope objective. In the BFP, the angle of the emission to the optical axis is directly visible. Figure 4d–f show BFP images of the nanofiber coupled with the hBN flake in three different configurations. First, in Figure 4d, in order to check the general scattering properties, broadband light from a halogen lamp is coupled into the fiber and the scattered light observed. Light leaking from the fiber is visible under high angles at the left side of the image. In addition, scattering from the particle hosting the hBN flake can be seen in the middle. Second, in Figure 4e, the BFP image is shown when exciting through the fiber. Due to contributions of other sources of light at other wavelengths, a near-isotropic emission is found. Finally, to investigate the light only from the single defect at 666 nm wavelength, in Figure 4f the fluorescence when using the 10 nm bandpass is shown. Two lobes are visible, separated by a minimum along the fiber axis. This situation can be compared to the numerical calculation shown in Figure 4g (see Methods).

In these calculations, the back focal plane intensity pattern is investigated for a dipole in parallel orientation at positions on top of the fiber, at the middle position, and at the bottom position (labeled 1–3, respectively). The data shown are normalized to each panel's maximum, and the fraction of the total emitted power falling in the numerical aperture of 0.95 used in the experiment is 0.22, 0.22, and 0.51, respectively. This shows that the position of the dipole has a dramatic effect on the number of photons that can be collected with an objective lens in free space that has to be taken into account when calculating the coupling efficiency to the nanofiber. The assumption of isotropic emission of the emitter, while often made, is a relatively coarse approximation, as we will investigate later in this paper. In our case, the pattern when the dipole sits at the middle of the fiber is closest to the measured result in Figure 4f. Hence, the calculated free space collection efficiency is $\eta_{\mathrm{obj,calc}} = 0.22$. In order to find the best resemblance of the experimental results, simulation results for all three dipole orientations and positions were compared, and a dipole orientation matching the polarization measurements was found. A more in-depth analysis of the far-field pattern for different dipole orientations goes beyond the scope of this paper and is left for future work.

The values found for the collection efficiency differ by more than a factor of 2 for different dipole positions. It is therefore

DOI: 10.1021/acsphotonics.7b00025
ACS Photonics 2017, 4, 761–767

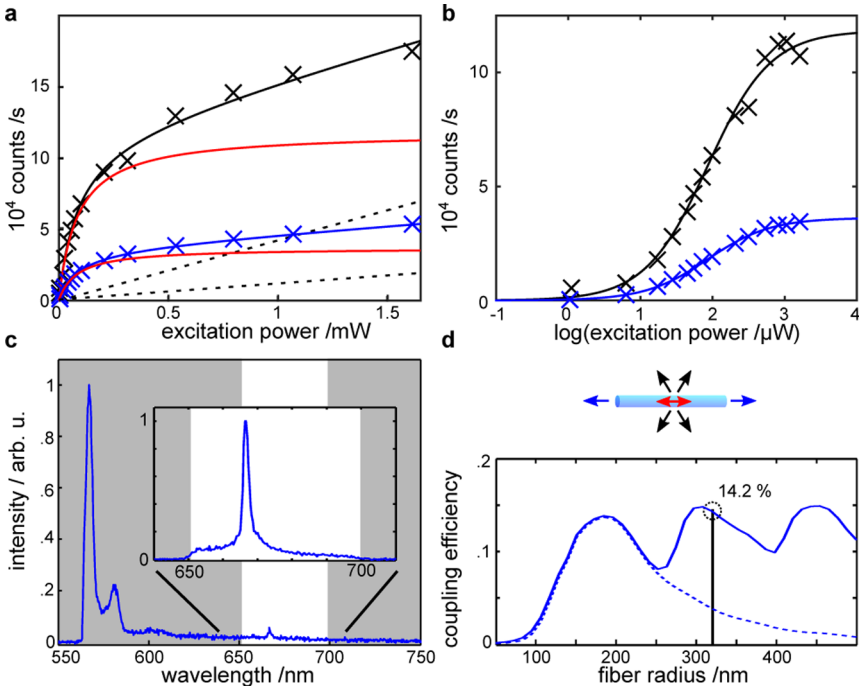

Figure 3. Saturation measurements and fiber coupling efficiency. (a) Saturation curve of the single defect coupled to the nanofiber measured collecting the light through the objective (black) and through the fiber (blue). The curves follow eq 1 with parameters $R_{inf,obj}$ = 118 kcounts/s, $I_{s,obj}$ = 86 μW, and BG_{obj} = 42 counts/μW for the black curve and $R_{inf,fib}$ = 36 kcounts/s, $I_{s,fib}$ = 86 μW, and BG_{fib} = 11 counts/μW for the blue curve, respectively. Integration time for each data point was 3 s, which is much longer than the blinking time scale in Figure 2f. The red curves are the contribution of the defect, whereas the dashed lines are the background contribution. (b) Representation of the data in panels a and b on a linear/logarithmic plot with background correction applied. (c) Spectrum collected when detecting and pumping through the fiber. Even though the pump light propagated through the fiber and excited background fluorescence, the defect at 666 nm is visible. The inset shows the signal after optimization of coupling of the pump light. Shaded areas are filtered out in the inset. (d) Simulation on the nanofiber diameter and coupling efficiency. The upper part shows a sketch of the geometry investigated, while the lower part shows the variation of the coupling into the fiber for a dipole with longitudinal orientation.

illustrative to compare them with the result when assuming isotropic emission of the dipole. In this case, the 0.95 NA collection lens collects $\eta_{obj,geom} \approx 34\%$ of the full solid angle. This would—using the value of $\eta_{fib,calc}$ = 14.2% for the coupling efficiency to the fiber from the calculations shown in Figure 3d—yield a value for the microscope collection efficiency of $\eta_{obj,iso} = (1 - \eta_{fib,calc}) \times 34\% = 0.29$.

In order to get an experimental value for the coupling efficiency in the fiber, the transmission of the optics has to be known (see Methods). Experimentally, we found a relative transmission for the two different paths of $t_{rel} = \frac{t_{obj}}{t_{fib}} = 0.72$. The coupling efficiency to the fiber η_{fib} is then given by

$$\eta_{fib} = \frac{R_{inf,fib} \times 2}{R_{inf,obj}} \times t_{rel} \times \eta_{obj,calc} = 10\% \quad (2)$$

where the factor of 2 accounts for the fact that light is emitted to both ends of the fiber.

This shows that the fiber coupled system is able to achieve a similar collection efficiency to a high-NA objective lens, while having the advantage of being directly fiber coupled, and offers alignment free collection. With the use of nanofiber Bragg cavities, this value can even surpass high-NA objective lenses, and efficiencies over 80% are expected.[26]

The value of the coupling efficiency of 10% found here is consistent with the findings of other results using other emitters such as quantum dots[21,22] or defect centers.[23,29] While those measurements were performed using a single-mode nanofiber, here a fiber in the multimode regime was used. In this regime the total coupling efficiency can be even higher than in the single-mode regime,[30,31] which can be seen in Figure 3d. The peak for small fiber diameters (single-mode regime) is smaller than the other two peaks for a larger radius.

In conclusion, we realized an integrated photonic system where a quantum emitter in a 2D material, layered hBN, is coupled to a tapered optical fiber. We achieved highly efficient coupling to the fiber with an efficiency of 10% and were able to prove the quantum nature of the light emitted. BFP imaging of the emission dipole and polarization measurements confirm the efficient coupling of the quantum emitter to the tapered fiber and show that the dipolar emission pattern of the emitter has to be taken into account when measuring the coupling efficiency. The highly efficient coupling observed even allows for excitation of the emitter and collection through the same fiber, establishing a fully fiber integrated system. Our results pave the way for promising applications in integrated quantum photonics using single emitters in hBN.

METHODS

hBN Samples. A native oxide Si(100) substrate was cleaned thoroughly with acetone, 2-propanol, and ethanol before drop-casting 100 μL of ethanol solution containing pristine hBN flakes (Graphene Supermarket) of approximately 200 nm in diameter and 5−50 nm in height onto silicon substrates. The completely dried sample was then loaded into a fused-quartz tube in a tube furnace (Lindberg Blue). The tube was evacuated

DOI: 10.1021/acsphotonics.7b00025
ACS Photonics 2017, 4, 761−767

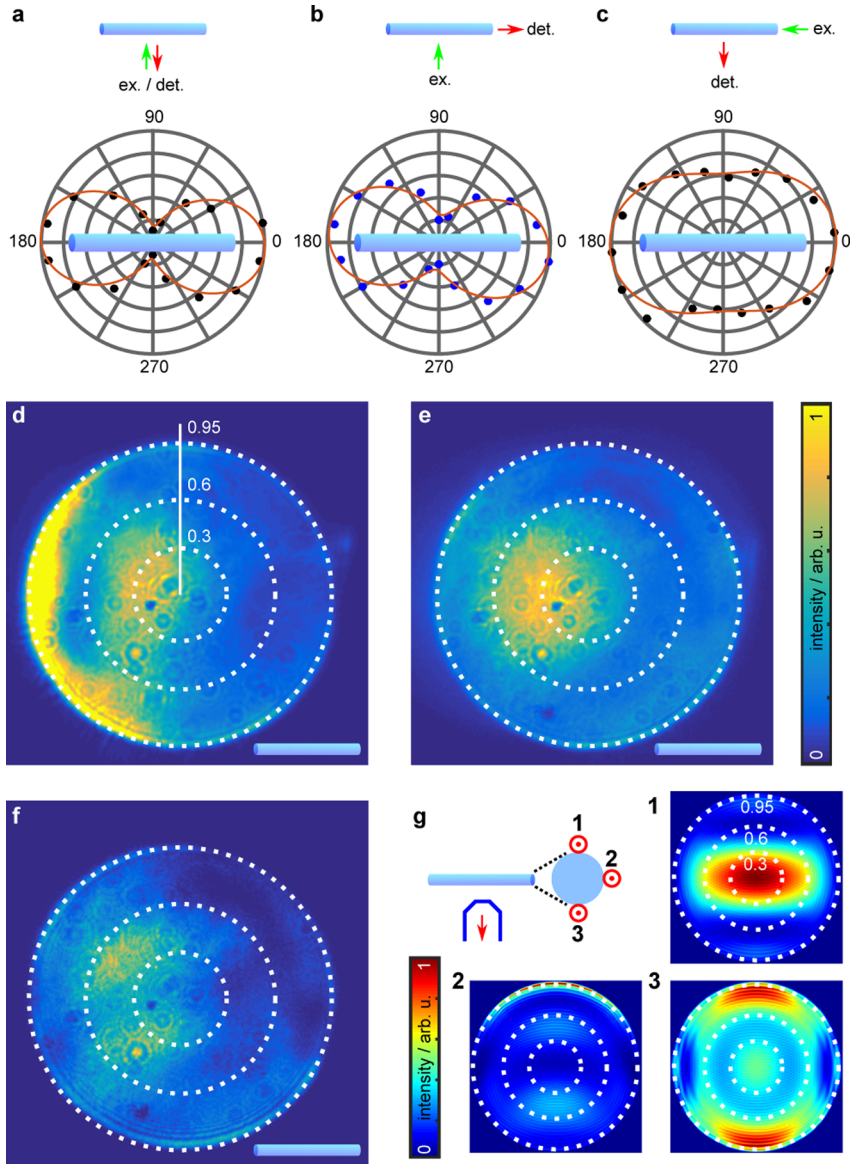

Figure 4. Polarization and back focal plane measurements. (a) Intensity of the emission measured through the objective when the excitation polarization is rotated. The fiber axis is horizontal from 0 to 180 deg. (b) Intensity of the emission as measured through the fiber. (c) Intensity collected through the objective when excited through the fiber. In contrast to panels a and b, not the excitation polarization, but the polarization of the detection is varied using a polarizer. (d) Back focal plane (BFP) image when white light from a halogen lamp (561 to 700 nm wavelength) is coupled into the fiber from the right side. Light leaking from the fiber can be seen on the left at high angles, while light scattered from the particle attached can be seen in the middle. (e) BFP image of the fluorescence when pumped through the fiber (561 to 700 nm wavelength). Since the excitation laser gets filtered out, no light leaking from the fiber can be detected. This situation corresponds to a near-isotropic emission; the offset to the left is due to a slight misalignment of the optics (also present in the other panels). (f) BFP image when the 10 nm bandpass filter is introduced. Two lobes are visibly separated by a minimum on the fiber axis. (g) Numerical calculations of the far-field pattern and the corresponding collection efficiency for different dipole positions (1: back side, 2: middle position, 3: front side). The best resemblance of the measured pattern was found for a longitudinal dipole at a position at the middle of the fiber. The fiber is oriented horizontally in all panels.

to low vacuum (10^{-3} Torr) by using a rough pump, then purged for 30 min under 50 sccm of Ar with pressure regulated at 1 Torr. The substrate was then annealed at 850 °C for 30 min under 1 Torr of argon. This thermal treatment step is employed to increase the optically active defect density.[32]

Tapered Fibers. The tapered fiber is fabricated by heating an optical fiber (0.25Z-U, Sumitomo Electric) with a ceramic heater to a temperature of about 1350 °C. The fiber was stretched for 200 s with speeds from 0.2 to 0.3 mm/s, resulting in an overall distance of 505 mm. With this, a waist diameter of about 640 nm was achieved. The transmission of the fiber stayed (apart from mode beating expected in multimode fibers) close to unity during this process.

Setup. The experimental setup used (shown in Figure 1) consists of a home-built confocal microscope and a manipulator. The manipulator consists of a sharp tungsten tip (TP-0002, Micro Support) and a three-axis piezo stage (TRITOR 100, Piezosystem Jena). The microscope objective used (MPlanApo N 100×/0.95, Olympus) has a numerical aperture of 0.95 and is mounted on a one-axis piezo stage (TRITOR 100 SG, Piezosystem Jena) to adjust the focus. Scanning is achieved by a scanning mirror unit (GVS002,

DOI: 10.1021/acsphotonics.7b00025
ACS Photonics 2017, 4, 761−767

Thorlabs), and the excitation lasers used are a 532 nm wavelength continuous wave laser (LBX-532, Oxxius) and a picosecond laser at the same wavelength (Katana, Onefive) for pulsed measurements. Detection is done via two avalanche photodiodes (SPCMM-AQRH-14-FC, PerkinElmer) behind a fiber beam splitter connected to a counting module (Time Harp 200, Picoquant) or by a Peltier cooled camera (DU420-OE, Andor) behind a monochromator (Oriel MS257). For back focal plane imaging, the back focal plane is imaged on a Peltier cooled camera (PIXIS 1024, Princeton Instruments). Transmissions of the microscope and fiber setup were measured to be 0.56 (without 10 nm bandpass filter, fiber in-coupling, and microscope objective) and 0.7 for the setup used for filtering the light from the fiber (not including fiber in- and out-coupling). The transmission of the bandpass filter cancels out, as it is used in both setups, and the difference in fiber coupling is estimated to be 90%. The transmission of the microscope objective is given as 90% by the manufacturer. The relative transmission is hence $t_{rel} = \frac{t_c}{t_f} = 0.72$.

FDTD Simulations. In order to analyze the far-field pattern and the corresponding collection efficiency, three-dimensional finite-difference time-domain (FDTD) simulations were performed on a commercial package (FDTD Solutions, Lumerical). The calculation region (length × width × height) was set to 40 μm × 40 μm × 4 μm. An automatic nonuniform mesh and the material properties of SiO_2 provided by the software were used in the calculation. A single-dipole source was slightly outside (0.5 nm) the surface of the fiber. Perfectly matched layers were employed as absorbing boundary conditions. The far-field pattern was calculated from the top side of the calculation region.

The coupling efficiency to the nanofiber is calculated by comparing the total emission of a dipole with the power coupled into the fiber measured with a 4 μm × 4 μm sized monitor at the end of the nanofiber.

AUTHOR INFORMATION

Corresponding Authors

*E-mail (A. W. Schell): aws.kyoto@gmail.com.
*E-mail (S. Takeuchi): takeuchi@kuee.kyoto-u.ac.jp.

ORCID

Igor Aharonovich: 0000-0003-4304-3935

Notes

The authors declare no competing financial interest.

ACKNOWLEDGMENTS

We thank Kali Nayak for help with the low-fluorescent nanofibers, Syun Suezawa for help with Figure 1, and Hironaga Maruya and Atsushi Fukuda for support. The work was further supported by MEXT/JSPS Kakenhi Grant Numbers 26220712 and 21102007, JST CREST project, and Special Coordination Funds for Promoting Science and Technology. A.W.S. thanks funding by the Japanese Society for the Promotion of Science through a fellowship for overseas researchers. Financial support from the Australian Research Council (IH150100028, DE130100592) and the Asian Office of Aerospace Research and Development Grant FA2386-15-1-4044 is gratefully acknowledged.

REFERENCES

(1) Mak, K. F.; Shan, J. Photonics and optoelectronics of 2D semiconductor transition metal dichalcogenides. *Nat. Photonics* **2016**, *10*, 216−226.
(2) Novoselov, K.; Mishchenko, A.; Carvalho, A.; Neto, A. C. 2D materials and van der Waals heterostructures. *Science* **2016**, *353*, aac9439.
(3) Wu, S.; Buckley, S.; Schaibley, J. R.; Feng, L.; Yan, J.; Mandrus, D. G.; Hatami, F.; Yao, W.; Vuckovic, J.; Majumdar, A.; Xu, X. Monolayer semiconductor nanocavity lasers with ultralow thresholds. *Nature* **2015**, *520*, 69−72.
(4) Caldwell, J. D.; Kretinin, A. V.; Chen, Y.; Giannini, V.; Fogler, M. M.; Francescato, Y.; Ellis, C. T.; Tischler, J. G.; Woods, C. R.; Giles, A. J.; Hong, M.; Watanabe, K.; Taniguchi, T.; Maier, S. A.; Novoselov, K. S. Sub-diffractional volume-confined polaritons in the natural hyperbolic material hexagonal boron nitride. *Nat. Commun.* **2014**, *5*, 5221.
(5) Dai, S.; Fei, Z.; Ma, Q.; Rodin, A. S.; Wagner, M.; McLeod, A. S.; Liu, M. K.; Gannett, W.; Regan, W.; Watanabe, K.; Taniguchi, T.; Thiemens, M.; Dominguez, G.; Castro Neto, A. H.; Zettl, A.; Keilmann, F.; Jarillo-Herrero, P.; Fogler, M. M.; Basov, D. N. Tunable phonon polaritons in atomically thin van der Waals crystals of boron nitride. *Science* **2014**, *343*, 1125−1129.
(6) Yang, W.; Shang, J.; Wang, J.; Shen, X.; Cao, B.; Peimyoo, N.; Zou, C.; Chen, Y.; Wang, Y.; Cong, C.; Huang, W.; Yu, T. Electrically Tunable Valley-Light Emitting Diode (vLED) Based on CVD-Grown Monolayer WS2. *Nano Lett.* **2016**, *16*, 1560−1567.
(7) Sie, E. J.; McIver, J. W.; Lee, Y.-H.; Fu, L.; Kong, J.; Gedik, N. Valley-selective optical Stark effect in monolayer WS2. *Nat. Mater.* **2015**, *14*, 290−294.
(8) Clark, G.; Schaibley, J. R.; Ross, J. S.; Taniguchi, T.; Watanabe, K.; Hendrickson, J. R.; Mou, S.; Yao, W.; Xu, X. Single Defect Light Emitting Diode in a van der Waals Heterostructure. *Nano Lett.* **2016**, *16*, 3944−3948.
(9) Withers, F.; Del Pozo-Zamudio, O.; Mishchenko, A.; Rooney, A.; Gholinia, A.; Watanabe, K.; Taniguchi, T.; Haigh, S.; Geim, A.; Tartakovskii, A.; S, N. K. Light-emitting diodes by band-structure engineering in van der Waals heterostructures. *Nat. Mater.* **2015**, *14*, 301−306.
(10) Tran, T. T.; ElBadawi, C.; Totonjian, D.; Lobo, C. J.; Grosso, G.; Moon, H.; Englund, D. R.; Ford, M. J.; Aharonovich, I.; Toth, M. Robust multicolor single photon emission from point defects in hexagonal boron nitride. *ACS Nano* **2016**, *10*, 7331−7338.
(11) Bourrellier, R.; Meuret, S.; Tararan, A.; Stephan, O.; Kociak, M.; Tizei, L. H.; Zobelli, A. Bright UV single photon emission at point defects in h-BN. *Nano Lett.* **2016**, *16*, 1317−4321.
(12) Jungwirth, N. R.; Calderon, B.; Ji, Y.; Spencer, M. G.; Flatt, M. E.; Fuchs, G. D. Temperature Dependence of Wavelength Selectable Zero-Phonon Emission from Single Defects in Hexagonal Boron Nitride. *Nano Lett.* **2016**, *16*, 6052−6057.
(13) Chejanovsky, N.; Rezai, M.; Paolucci, F.; Kim, Y.; Rendler, T.; Rouabeh, W.; Favaro de Oliveira, F.; Herlinger, P.; Denisenko, A.; Yang, S.; Gerhardt, I.; Finkler, A.; Smet, J. H.; Wrachtrup, J. Structural Attributes and Photodynamics of Visible Spectrum Quantum Emitters in Hexagonal Boron Nitride. *Nano Lett.* **2016**, *16*, 7037−7045.
(14) Schell, A. W.; Tran, T. T.; Takashima, H.; Takeuchi, S.; Aharonovich, I. Non-linear excitation of quantum emitters in hexagonal boron nitride multiplayers. *APL Photonics* **2016**, *1*, 091302−091302.
(15) Helmchen, F.; Denk, W. Deep tissue two-photon microscopy. *Nat. Methods* **2005**, *2*, 932−940.
(16) Gaponenko, S. V. *Introduction to Nanophotonics*; Cambridge University Press, 2010.
(17) Weber, J.; Koehl, W.; Varley, J.; Janotti, A.; Buckley, B.; Van de Walle, C.; Awschalom, D. D. Quantum computing with defects. *Proc. Natl. Acad. Sci. U. S. A.* **2010**, *107*, 8513−8518.
(18) Aharonovich, I.; Englund, D.; Toth, M. Solid-state single-photon emitters. *Nat. Photonics* **2016**, *10*, 631−641.

DOI: 10.1021/acsphotonics.7b00025
ACS Photonics 2017, 4, 761−767

(19) Mansfield, S. M.; Kino, G. S. Solid immersion microscope. *Appl. Phys. Lett.* **1990**, *57*, 2615−2616.
(20) Lee, K. G.; Chen, X. W.; Eghlidi, H.; Kukura, P.; Lettow, R.; Renn, A.; Sandoghdar, V.; Gotzinger, S. A planar dielectric antenna for directional single-photon emission and near-unity collection efficiency. *Nat. Photonics* **2011**, *5*, 166−169.
(21) Yalla, R.; le Kien, F.; Morinaga, M.; Hakuta, K. Efficient channeling of fluorescence photons from single quantum dots into guided modes of optical nanofiber. *Phys. Rev. Lett.* **2012**, *109*, 063602−063602.
(22) Fujiwara, M.; Toubaru, K.; Noda, T.; Zhao, H.-Q.; Takeuchi, S. Highly Efficient Coupling of Photons from Nanoemitters into Single-Mode Optical Fibers. *Nano Lett.* **2011**, *11*, 4362−4365.
(23) Liebermeister, L.; Petersen, F.; Munchow, A. v.; Burchardt, D.; Hermelbracht, J.; Tashima, T.; Schell, A. W.; Benson, O.; Meinhardt, T.; Krueger, A.; Stiebeiner, A.; Rauschenbeutel, A.; Weinfurter, H.; Weber, M. Tapered fiber coupling of single photons emitted by a deterministically positioned single nitrogen vacancy center. *Appl. Phys. Lett.* **2014**, *104*, 031101−031101.
(24) Yalla, R.; Sadgrove, M.; Nayak, K. P.; Hakuta, K. Cavity quantum electrodynamics on a nanofiber using a composite photonic crystal cavity. *Phys. Rev. Lett.* **2014**, *113*, 143601−143601.
(25) Schell, A. W.; Takashima, H.; Kamioka, S.; Oe, Y.; Fujiwara, M.; Benson, O.; Takeuchi, S. Highly efficient coupling of nanolight emitters to a ultra-wide tunable nanofibre cavity. *Sci. Rep.* **2015**, *5*, 9619−9619.
(26) Takashima, H.; Fujiwara, M.; Schell, A. W.; Takeuchi, S. Detailed numerical analysis of photon emission from a single light emitter coupled with a nanofiber Bragg cavity. *Opt. Express* **2016**, *24*, 15050−15058.
(27) Fujiwara, M.; Yoshida, K.; Noda, T.; Takashima, H.; Schell, A. W.; Mizuochi, N.; Takeuchi, S. Manipulation of single nanodiamonds to ultrathin fiber-taper nanofibers and control of NV-spin states toward fiber-integrated lambda-systems. *Nanotechnology* **2016**, *27*, 455202−455202.
(28) Novotny, L.; Hecht, B. *Principles of Nano-optics*; Cambridge University Press, 2012.
(29) Schroeder, T.; Fujiwara, M.; Noda, T.; Zhao, H.-Q.; Benson, O.; Takeuchi, S. A nanodiamond-tapered fiber system with high single-mode coupling efficiency. *Opt. Express* **2012**, *20*, 10490−10497.
(30) Kumar, R.; Gokhroo, V.; Deasy, K.; Maimaiti, A.; Frawley, M. C.; Phelan, C.; Chormaic, S. N. Interaction of laser-cooled 87Rb atoms with higher order modes of an optical nanofibre. *New J. Phys.* **2015**, *17*, 013026.
(31) Shi, Q.; Sontheimer, B.; Nikolay, N.; Schell, A.; Fischer, J.; Naber, A.; Benson, O.; Wegener, M. Wiring up pre-characterized single-photon emitters by laser lithography. *Sci. Rep.* **2016**, *6*, 31135−31135.
(32) Tran, T. T.; Bray, K.; Ford, M. J.; Toth, M.; Aharonovich, I. Quantum emission from hexagonal boron nitride monolayers. *Nat. Nanotechnol.* **2016**, *11*, 37−41.

DOI: 10.1021/acsphotonics.7b00025
ACS Photonics 2017, 4, 761−767